Self-assembled Growth of Coaxial Crystalline Nanowires

Ghim W. Ho,[†] Andrew S. W. Wong,[‡] Andrew T. S. Wee,[§] and Mark E. Welland*,[†]

Nanoscience Centre, University of Cambridge, 11 J. J. Thomson Avenue, Cambridge, CB3 0FF, United Kingdom, Department of Materials Science and Metallurgy, University of Cambridge, Pembroke Street, Cambridge, CB2 3QZ, United Kingdom, and Department of Physics and NUS Nanoscience and Nanotechnology Initiative, National University of Singapore, 2 Science Drive 3, Singapore 117542

ABSTRACT

Coaxial crystalline nanowires have been synthesized by chemical vapor deposition. Recrystallization of a copper substrate provided a natural template for the self-assembled growth of nanowires. The core of the wires is made up of numerous faceted SiC nanowires typically 20–50 nm in diameter, encapsulated by larger hollow wires typically 0.2–1.0 μm in diameter. The nanowires are crystalline and catalyst free. A vapor–solid growth mechanism is proposed based on detailed morphology and structural characterization.

Accompanying the dimensional miniaturization of silicon-based semiconductor devices, it is desirable to create a new class of nanowire material that is compatible with existing integrated circuit fabrication processes.[1−5] The bottom-up self-assembly approach to fabricate silicon-based nanomaterials rather than the traditional top-down approach, inherent in traditional lithography techniques, is becoming of increasing interest.[6−9] Here we report, for the first time, the fabrication of self-assembled coaxial crystalline nanowires. Thermal treatment of a polycrystalline copper substrate prior to vapor phase deposition caused thermal grooving along grain boundaries. These exposed grain boundaries then provided a natural template for the self-assembled growth of the nanowires during the vapor phase growth process. Numerous faceted nanowires were observed to be encapsulated within a larger diameter hollow wire, and other composite nanocrystals were also found to nucleate randomly on the sheath of the wires. The combination of one-dimensional self-assembled nanowires and zero-dimensional nanocrystals may lead to novel and exciting nanomaterials with important applications in nanotechnology.

Si was placed at the center of a horizontal tube furnace while Cu foil was placed downstream to collect the vaporized material. The deposition system was then pumped down to $\sim 3 \times 10^{-6}$ Torr. The temperature of the tube furnace was then ramped to 1180 °C with argon gas admitted as the background gas, the pressure being maintained at $\sim$10 Torr. When the deposition temperature (1180 °C) was attained, 300 sccm methane gas was admitted for 30 min at $\sim$10 Torr. Finally, the chamber was cooled to room temperature in an argon ambient. The morphology, structure, and chemical properties of the synthesized nanowires were characterized using a field-emission LEO 1530 VP scanning electron microscope (SEM), FEI CM300 field emission transmission electron microscope (FEGTEM), and a ESCALAB220I-XL X-ray photoelectron spectroscopy system (XPS).

Figure 1a shows the SEM image of a Cu foil after initial thermal annealing at 1000 °C in an argon atmosphere. The foil clearly shows the presence of grains $\sim$0.2−2 μm in diameter with some evidence of thermal grooving indicating thermally activated mass transport of the copper. Immediately after the methane gas is introduced, numerous isolated nanocrystals $\sim$20−50 nm are observed to nucleate on the Cu foil (Figure 1b). These nanocrystals coalesce along the grain boundaries (Figure 1c) and exhibit a strong texturing with a hexagonal symmetry. Sintering of the nanocrystals is observed to occur along the grain boundaries. Neighboring nanocrystals fuse "side-on" forming elongated walls or, alternatively, can also meet "corner-to-corner" creating a sharp edge configuration. Thus, the existence of exposed grain boundaries on the Cu foil has provided many high energy sites which promote grain boundary induced diffusion and migration between nanocrystals.[10] Both interstitials and

* Corresponding author. E-mail: mew10@cam.ac.uk.
† Nanoscience Centre, University of Cambridge.
‡ Department of Materials Science and Metallurgy, University of Cambridge.
§ National University of Singapore.
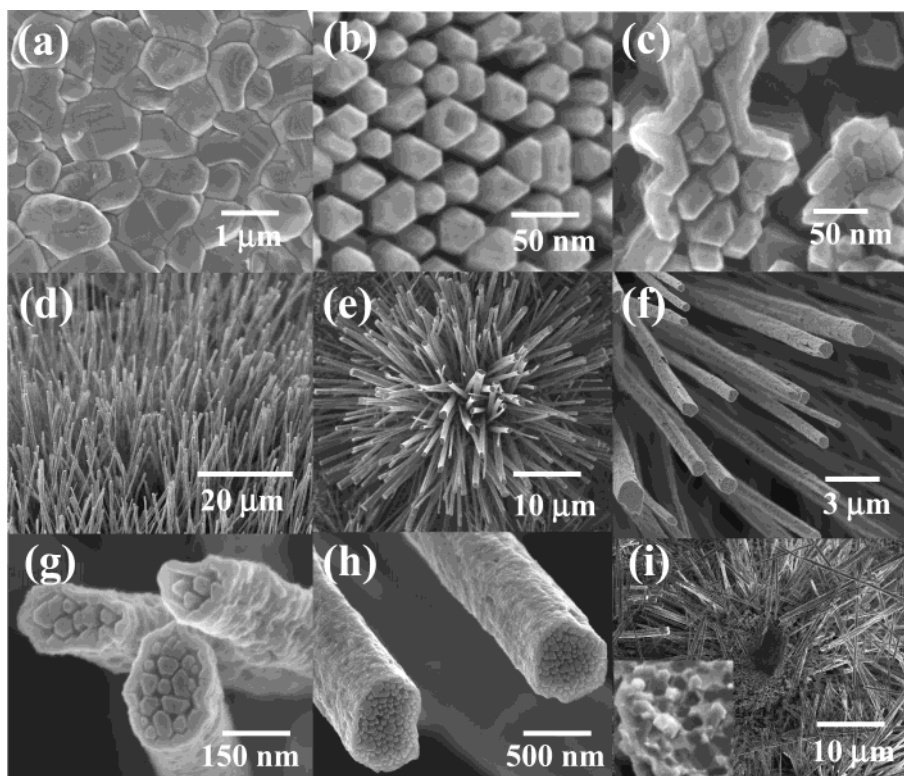
Figure 1. SEM image of (a) numerous well-defined grain boundaries on the Cu foil film after Ar annealing at 1000 °C; (b) facetted nanocrystals deposited on Cu foil after methane gas exposure; (c) nanocrystals sintering/coalescing along the grain boundaries, forming an enclosed nanocrystal edge; (d) as-synthesized array of vertically aligned nanowires; (e) a bunch of nanowires growing radially with a bush-like structure; (f) flat nanowire tips without any evidence of attached metal catalyst; (g−h) close view of tips with various diameters showing numerous nanowires encapsulated within wires; (i) the bunch of nanowires in Figure 1e after cutting the nanowires cross-sectionally with a scalpel. Inset: cross-sectional view of an array of nanowires revealing the multi-coaxial profile.

vacancies are known to play important roles in grain-boundary mass transport via a Frenkel pair generation process.[11]

After the initial nanocrystal nucleation, the incident precursor gas molecules preferentially deposit on top of these nanocrystals since the incoming flux can no longer reach the valleys between the nanocrystals due to the shadowing effect.[12] Consequently, the isolated nanocrystals grow normal to the substrate surface to form complex nanowire structures. Such unidirectional growth will continue as long as a favorable gas ambient is maintained. Figures 1d−e show an array of as-synthesized vertically aligned densely packed nanowires and a bunch of nanowires sprouting radially. These nanowires grow up to tens of microns in length without branching or entanglement. The tips of the nanowires are observed to be flat without any evidence of catalyst particles (Figure 1f). Close inspection of the nanowire tips shows numerous nanowires enclosed within a larger diameter wire, and the number of enclosed nanowires varies from 3 to 200, depending on the diameter (typically 0.2−2 μm) of the encapsulating wire (Figures 1g−h). Figure 1i shows a cross section of the nanowire structures obtained after cleaving the substrate with a scalpel. The inset image in Figure 1i shows the cross-sectional view of a broken nanowire revealing its multi-coaxial profile, indicating that the faceted

nanowires within each hollow wire maintain their integrity along the whole length of the nanowire.

The TEM image in Figure 2a reveals numerous columnar crystalline nanowire cores (with darker contrast) within the encapsulating nanowire. The crystalline nanowire core is grown such that its *c*-axis is oriented along the longitudinal axis of the encapsulating nanowire. The TEM image indicates that the nucleation and growth of the nanowire cores are not random but confined within the encapsulating nanowire. The diameters of the crystalline nanowire cores and the encapsulating nanowire are approximately 20−40 and 220 nm respectively, in agreement with the SEM observations.

Figure 2b taken at the core of the nanowire (indicated by a circle) reveals a high density of planar defects inclined to the axis of the nanowires; characteristic of SiC stacking faults.[13] The high-resolution TEM image in Figure 2c confirms a crystalline SiC nanowire core with an interplanar spacing of 0.25 nm, and the selected area electron diffraction (SAED) pattern recorded along the $\langle 110 \rangle$ zone axis reveals the {111} β-SiC crystal planes.[14,15] CuO nanocrystals and disordered graphite are also randomly observed on the contours of the amorphous sheath in figures 2d and e, respectively. The CuO nanocrystals have an interplanar spacing of 0.23 nm corresponding to the calculated {111} planes of monoclinic CuO.[16] The vapor solid mechanism is responsible for producing CuO vapor from native oxide
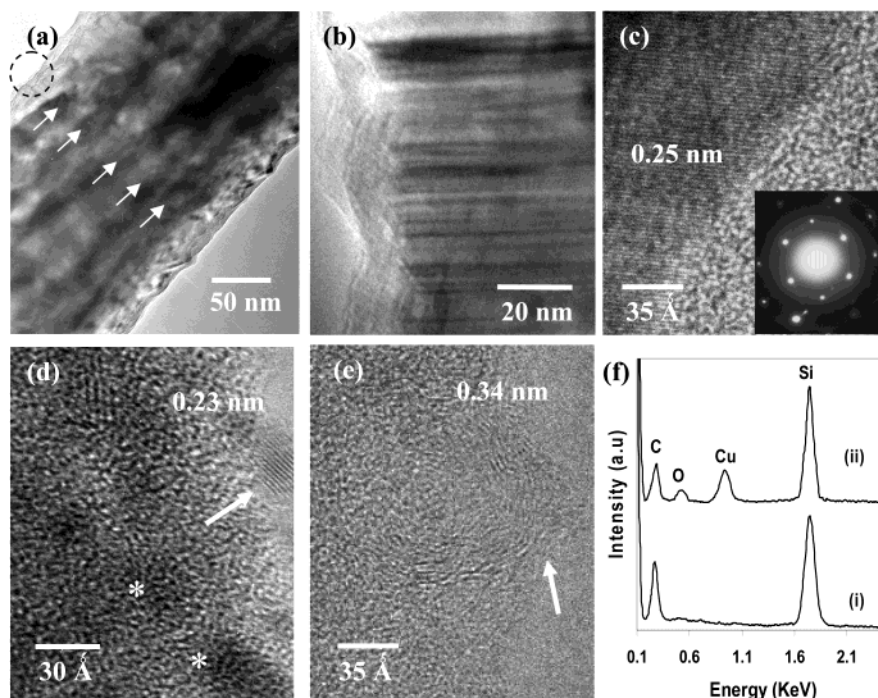
Figure 2. (a) TEM image of a multi-coaxial wire exhibiting columnar nanowires (indicated by arrows) with their axes lying along the $\langle 111 \rangle$ direction. (b) Higher magnification TEM reveals planar defects, stacking faults aligned perpendicular to the axis, generally thought to originate from thermal stress during the growth process. (c) High-resolution TEM confirms the interplanar distance to be consistent with the {111} planes of β-SiC, and the inset shows the SAED pattern recorded along the $\langle 110 \rangle$ zone axis with the extra streaks attributed to twinning. (d) CuO nanocrystals are seen to nucleate on the surface (indicated by arrow) and beneath the surface (indicated by asterisks) of the amorphous sheath. (e) Disordered graphitic sheets (interplanar spacing 0.34 nm) are also observed on the sheath of the nanowire. (f) EDX spectra measured at the (i) core and (ii) sheath of the nanowire. XPS was used to provide surface chemical information of the multi-coaxial nanowires.

coated Cu foil, which deposited as nanocrystals on nanowire sheaths.[16] The existence of disordered graphite along the sheath may be explained by the nucleation and crystallization of unreacted residual carbonaceous gas.[17] Furthermore, hydrogen from decomposed methane gas may help to maintain hybridization of carbon, seeding graphite nanocrystal growth.[18] Elementary analysis from selected area energy-dispersive X-ray (EDX) in Figure 2f confirms the constitution of the nanowires. EDX spectrum (i) taken at the core of the nanowires shows Si and C peaks, while spectrum (ii) taken at the sheath of the nanowires in Figure 2d shows Si, C, Cu, and O peaks. On the basis of SEM and TEM observations, the vapor−liquid−solid (VLS) mechanism may not be able to fully explain the growth mechanism of the nanowires since the solid-phase reactant silicon was used and no catalyst particles were found on the grown nanowires. Thus a vapor−solid nucleation mechanism is proposed.[21] First, vapor-phase SiC radicals are produced when the decomposed methane gas ($CH_4 \rightarrow C + 2H_2$) reacts with Si ($C + 2H_2 + Si \rightarrow SiC + 2H_2$). Silyl radicals from Si may be produced via a hydrogen mediated etching process.[22] Condensation of the SiC occurs on the surface of Cu foil at thermally exposed grain boundaries whereby spontaneous nucleation leads to the growth of the nanowires.

Figure 3a shows a high-resolution XPS C 1s spectrum from the as-synthesized nanowires and a reference graphite film. The C 1s spectrum of the nanowires shows three peak positions at 283.5, 284.3, and 285.4 eV which are assigned to C−Si, graphite, and graphitic carbon, respectively.[19,20] In comparison, the graphite film shows an absence of the C−Si peak at 283.3 eV. Figure 3b shows the Si 2p peak at 100.3 eV which corresponds to Si 2p binding energy of SiC, which is distinct from elemental Si 2p at a peak position of 99.3 eV.[20]

In summary, the synthesis of the self-assembled multi-coaxial nanowires within wires has been demonstrated. High mobility reactant gas species nucleate SiC nanocrystals at the grain boundaries, and subsequent sintering of the nanocrystals results in the formation of well-defined grain boundary nanocrystallites. Growth rates and diffusion kinetics depend on a number of parameters including temperature, crystallite size, surface wetting, and supporting substrate. The unique structures that evolve underline the importance of establishing a greater control and understanding of nucleation and growth processes of a range of nanowires. Here, the use of grain boundaries as nucleation sites has effected a singular morphology on the resulting SiC nanocrystals. This morphology, in turn, may have significant consequences in the range of applications that such materials may be useful for. The strongly geometric shape, high aspect ratio, and nanometer-scale cross section can, in combination, be expected to affect optical and electronic properties through confinement effects. When such materials are used in combination with conduct-

(a)

(b)
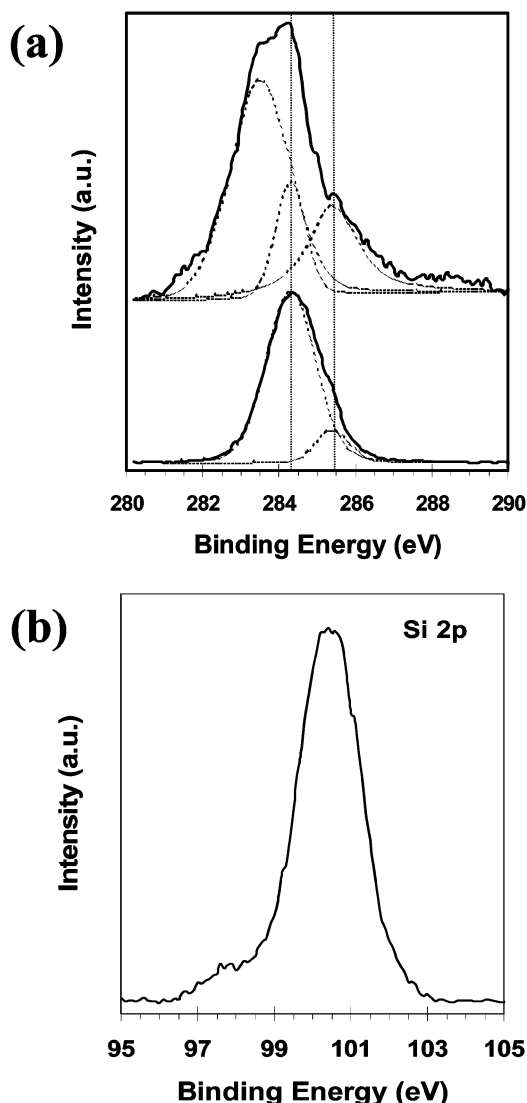
Figure 3. (a) In comparison to the graphite film, the XPS C1s spectrum of the nanowire shows an extra peak at 283.5 eV which is attributed to C−Si. (b) Si 2p spectrum shows a peak at 101.1 eV, which corresponds to Si 2p binding energy of SiC.

ing polymers to make a composite structure, there arepotential applications as a photovoltaic material. With further control of the growth parameters, so that nucleation site and growth orientation can be designed, there may be further applications as interconnects in functional devices.

References

(1) Hu, J. T.; Ouyang, M.; Yang, P. D.; Lieber, C. M. *Nature* **1999**, *399*, 48−51.
(2) Duan, X. F.; Niu, C. M.; Sahi, V.; Chen, J.; Parce, J. W.; Empedocles, S.; Goldman, J. L. *Nature* **2003**, *425*, 274−278.
(3) Barnett, R. N.; Landman, U. *Nature* **1997**, *387*, 788−791.
(4) Fasol, G. *Science* **1998**, *280*, 545−546.
(5) Whitney, T. M.; Jiang, J. S.; Searson, P. C.; Chien, C. L. *Science* **1993**, *261*, 1316−1319.
(6) Lopes, W. A.; Jaeger, H. M. *Nature* **2001**, *414*, 735−738.
(7) Wilson, J. N.; Bangcuyo, C. G.; Erdogan, B.; Myrick, M. L.; Bunz, U. H. F.; *Macromolecules* **2003**, *36*, 1426−1428.
(8) Zhang, H. F.; Dohnalkova, A. C.; Wang, C. M.; Young, J. S.; Buck, E. C.; Wang, L. S. *Nano Lett.* **2002**, 2, 105−108.
(9) Li, M.; Schnablegger, H.; Mann, S. *Nature* **1999**, *402*, 393−395.
(10) Nucci, J. A.; R. Keller, R. D.; Field, P.; Shacham-Diamand, Y. *Appl. Phys. Lett.* **1997**, *70*, 1242−1244.
(11) Liu, C. L.; Liu, X. Y.; Borucki, L. J. *Appl. Phys. Lett.* **1999**, *74*, 34−36.
(12) Karabacak, T.; Singh, J. P.; Zhao, Y. P.; Wang, G. C.; Lu, T. M. *Phys. Rev. B* **2002**, *68*, 125408−125412.
(13) Dai, H. J.; Wong, W. W.; Lu, Y. Z.; Fan, S.; Lieber, C. M. *Nature* **1995**, *375*, 769−772.
(14) Zhang, Y.; Suenaga, K.; Colliex, C.; Iijima, S. *Science* **1998**, *281*, 973−975.
(15) Wei, B. Q.; Ward, J. W.; Vaijtai, R.; Ajayan, P. M.; Ma, R.; Ramanath, G. *Chem. Phys. Lett.* **2002**, *354*, 264−268.
(16) Jiang, X. C.; Herricks, T.; Xia, Y. N. *Nano Lett.* **2002**, *2*, 1333−1338.
(17) Zhang, G. Y.; Jiang, X.; Wang, E. *Science* **2003**, *300*, 472−474.
(18) Welz, S.; Gogotsi, Y.; Mcnallan, M. J. *J. Appl. Phys.* **2003**, *93*, 4207−4214.
(19) Woo, H. K.; Lee, C. S.; Bello, I.; Lee, S. T. *Diamond Relat. Mater.* **1999**, *8*, 1737−1740.
(20) Shen, G. Z.; Chen, D.; Tang, K. B.; Qian, Y. T.; Zhang, S. Y. *Chem. Phys. Lett.* **2003**, *375*, 177−184.
(21) Yen, M. Y.; Chiu, C. W.; Hsia, C. H.; Chen, F. R.; Kai, J. J. Lee, C. Y.; Chiu, H. T. *Adv. Mater.* **2003**, *15*, 235−237.
(22) (22) Sharma, S.; Sunkara, M. K. *Nanotechnology* **2004**, *15*, 130−134.

NL0491733